Single and mechanically coupled capacitive silicon nanomechanical resonators

Nguyen Van Toan[1] ✉, *Tsuyoshi Shimazaki*[2], *Takahito Ono*[2]

[1]*Microsystem Integration Center (μSIC), Tohoku University, Sendai, Japan*
[2]*Graduate School of Engineering, Tohoku University, Sendai, Japan*
✉ *E-mail: nvtoan@nme.mech.tohoku.ac.jp*

Published in Micro & Nano Letters; Received on 9th May 2016; Revised on 3rd July 2016; Accepted on 15th July 2016

The design, fabrication and evaluation of single and mechanically coupled capacitive silicon nanomechanical resonators is reported. The structure of resonators is fabricated on a silicon on insulator wafer and transferred to a Tempax glass substrate by anodic bonding. A finite element method simulation has been conducted to investigate the vibration modes of the resonators. Single beam resonator with a length of 21.3 μm, a width of 500 nm, a thickness of 5 μm and the capacitive gap size of about 300 nm shows a nonlinear response. The amplitude of frequency response increases as the frequency is swept upward, and then suddenly jumps to a lower value. The mechanically coupled capacitive silicon nanomechanical resonator with a number of 100 individual beams above is successfully fabricated. Some resonant peaks can be observed, which shows that most nanomechanical resonators are mechanically coupled and synchronised. A mechanical resonance at a high frequency of ~7.2 MHz in flexural mode has been detected. A small motional resistance of 1.2 kΩ has been achieved by the mechanical coupling.

1. Introduction: Silicon micro/nanomechanical resonators have been studied for a wide range of applications [1–7] such as timing devices [1–3] in oscillation circuits for modern data and communication applications, high sensitive sensor [4–6], quantum information processing [7] and so on. The major advantages are its small mass, high frequency, low intrinsic dissipation, feasibility of integration with IC technology and so on. One of the simplest and most common methods to detect the motion of microfabricated resonators is based on the measurement of the change in capacitance between a sensing electrode and the resonant body [8–10]. However, this method may not be effective for nanomechanical resonators because of their very small change of motional capacitance. In addition, nanomechanical resonator has a large motional resistance, and hence, a high insertion loss that makes it difficult for practical applications. Generally, the motional resistance should be as small as possible. Therefore, the method for attaining a low motional resistance would be highly desirable.

To achieve a low motional resistance, investigations should be taken to improve the coupling efficiency. The narrowing the capacitive gap is by far the most effective, with a fourth power dependence [1, 11]. The different approaches to realise narrow capacitive gaps in silicon resonators are investigated in [12–14]. Resonator structures with a solid-filled gap are presented in [12]. The capacitive gap reduction by electrostatic force is reported in [13]. A fabrication method using a thin oxide film as a sacrificial layer has been presented in [14]. Besides efforts to reduce the capacitive gap size, development of arrays of nanomechanical resonator is also one of solutions for low motional resistance. An array of 20, 49 and 100 resonators has been designed and fabricated in [15] then all individual devices are electrically interconnected. The low motional resistances have been achieved; however, it may face with a large parasitic capacitance and the mismatch of the resonant frequencies that result in difficulty in capacitive detection.

In this research, mechanically coupled capacitive silicon nanomechanical resonators with 100 individual beams are fabricated and evaluated. The both-side clamped beams resonators are mechanically connected to neighbouring resonator by coupling silicon beams. The mechanical resonance properties and synchronisation performance are evaluated.

2. Device structure and working principle: The single beam nanomechanical resonator (device #1) is shown in Fig. 1*a*. It basically consists of silicon resonant body, driving/sensing electrodes and capacitive gaps. The resonator is electrically exited and vibrated at flexural mode by the combined influence of DC and AC actuation voltages (V_{DC} and V_{AC}). The output voltage of the resonator results from the changes in the capacitive gap on the sensing electrode. In turn, designed mechanically coupled nanomechanical resonator (device #2) is consisted of 100 single nanomechanical resonators connected by mechanically coupled elements, as shown in Fig. 1*b*. The summarised design parameters of devices #1 and #2 are shown in Table 1.

A finite element method (FEM) simulation is performed to demonstrate the vibration modes as shown in Figs. 1*c* and *d*. Device #1 vibrates at flexural mode as given in Fig. 1*c* and a synchronisation of mechanical elements indicates for device #2. Due to the limitation of memory of PC, we just perform the FEM simulation for 44 resonant body beams and 43 mechanical coupled beams as shown in Fig. 1*d*. Its vibration synchronises because of mechanical interaction via the vibration of the coupling element connecting those resonators.

Each resonator is represented by a mass-spring-damper system, while the coupling beam corresponds to a network of mechanical springs. Its electrical equivalent circuit can be drawn as shown in Fig. 2. The motional resistance R_m represents mechanical losses of vibration. The motional inductance L_m indicates mechanical inertia. The motional capacitance C_m corresponds to mechanical compliance. The motional parameters of the single capacitive resonator without coupling can be calculated by following equations [16–18]:

$$R_m = \frac{\sqrt{k_{eff} m_{eff}}}{Qn^2} = \frac{\sqrt{6.08E\rho}g^4}{QV_{DC}^2\varepsilon_0^2}\frac{W^2}{L^3 t}, \quad (1)$$

$$C_m = \frac{n^2}{k_{eff}} = \frac{V_{DC}^2\varepsilon_0^2}{16Eg^4}\cdot\frac{L^5 t}{W^3}, \quad (2)$$

$$L_m = \frac{m_{eff}}{n^2} = \frac{0.38\rho g^4}{V_{DC}^2\varepsilon_0^2}\cdot\frac{W}{Lt}, \quad (3)$$

where W is the width of resonant body, L is the length of resonant body, t is the thickness of device layer, g is the capacitive gap width, ε_0 is the electric constant ($\varepsilon_0 = 8.854 \times 10^{-12}$ Fm^{-1}), and E and ρ

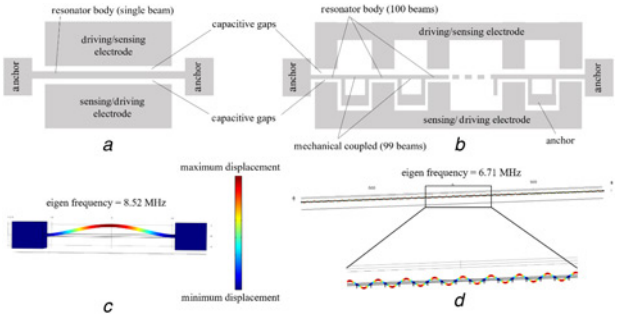

Fig. 1 *Device structures and FEM simulations*
a Single capacitive silicon nanomechanical resonator
b Mechanical coupled capacitive silicon nanomechanical resonator
c FEM simulation of single capacitive resonator
d FEM simulation of mechanical coupled capacitive resonator

Table 1 Summarised parameters of single and mechanically coupled capacitive silicon nanomechanical resonators

Parameters	Single (device #1)	Coupled (device #2)
width of resonant body (W)	500 nm	500 nm
length of resonant body (L)	21.3 μm	21.3 μm
SOI wafer		
• device layer (t) (resonator height)	5 μm	5 μm
• buried SiO_2 layer	0.4 μm	0.4 μm
• silicon handling layer	546 μm	546 μm
capacitive gap (g)	300 nm	300 nm
number of resonators	1	100
number of couplings	0	99
V_{DC}	10 V	15 V
V_{AC}	0 dBm	0 dBm
measured frequency (f_0)	9.9 MHz	7.2 MHz
amplitude peak (A)	0.5 dB	20 dB
quality factor (Q)	nonlinear	1000
motional resistance (R_m)	response	1.2 kΩ

are Young's modulus and density of structure material, respectively. n presents the electromechanical conversion factor between the mechanical and electrical domains. k_{eff} and m_{eff} are the effective spring constant and mass, respectively,

$$n = V_{\text{DC}} \frac{\varepsilon_0 Lt}{g^2}, \tag{4}$$

$$k_{\text{eff}} = 16E \frac{W^3 t}{L^3}, \tag{5}$$

$$m_{\text{eff}} = 0.38\rho LWt, \tag{6}$$

where ρ is the density of the silicon material.

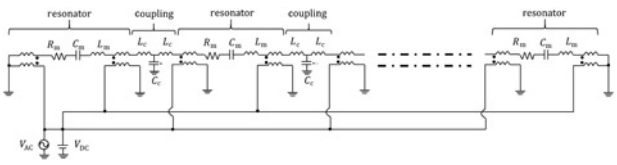

Fig. 2 *Electrical equivalent circuit of the mechanical coupled capacitive nanomechanical resonator*

The motional resistance can be manipulated by increasing the polarisation voltage V_{DC}, increasing Q factor, decreasing the capacitive gap width or increasing the overlap area of capacitance. Resonators can vibrate easily if the motional resistance is small and the motional capacitance is large. One of the simplest methods to achieve above two requirements is the increasing electrode to the resonator overlap area as shown in (1) and (2). Some research studies have investigated on this issue, such as the capacitive coupling of bulk acoustic wave silicon resonators [19] or mechanically corner-coupled square resonator array [20] and so on. The significant advantage of an array of coupling resonator by increasing overlap area provided over individual resonator.

In turn, mechanical coupling the nth number of resonators would be achieved by the design, here each resonator is designed in the same parameters and fabricated at the same time and process. It is expected to have the same resonant frequency. Hence, the lowering the effective motional resistance by the numbers of resonator can be achieved. The total motional resistance can be given by [20]

$$R_{\text{total}} = \frac{R_{\text{m}}}{n} \tag{7}$$

The resonant frequency f_0 of the clamped-clamped beam is calculated using following equation

$$f_0 = \frac{1}{2\prod}\sqrt{\frac{k_{\text{eff}}}{m_{\text{eff}}}} = 1.03\sqrt{\frac{E}{\rho}}\frac{W}{L^2} \tag{8}$$

A resonant frequency by FEM simulation of device #1 is 8.52 MHz, while that of device # 2 is 6.71 MHz. The possible reason caused this phenomenon is due to the mode splitting. However, the resonators will still be vibrating in unison at the same frequency as they are mechanically coupled. The shifting resonant frequency of each resonator caused by the effect of the spring constant of coupling k_{coupling} can be calculated by the equation below

$$w_n = \sqrt{\frac{1}{m}\left(k_1 + 2k_2\left(1 - \cos\frac{2\prod j}{n}\right)\right)} \tag{9}$$

with $j = 0, 1, 2, \ldots, n-1$.

3. Experiments

3.1. Device fabrication: Resonator structures are fabricated by following the fabrication process shown in Fig. 3. The fabrication process of details is as follows.

A silicon on insulator (SOI) wafer which consists of a 5 μm-thick top silicon layer, 0.4 μm-thick oxide layer and a 546 μm-thick silicon handling layer has been employed (Fig. 3*a*). A 300

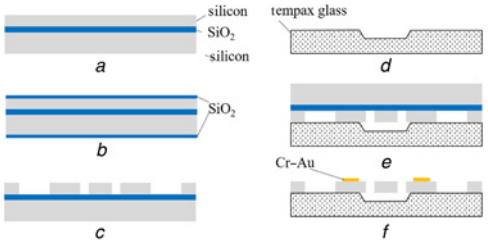

Fig. 3 *Fabrication process*
a SOI wafer
b Thermal oxidation
c Deep RIE
d Wet etching
e Anodic bonding
f Handling and SiO_2 layer removal and Cr–Au electrodes

doi: 10.1049/mnl.2016.0265

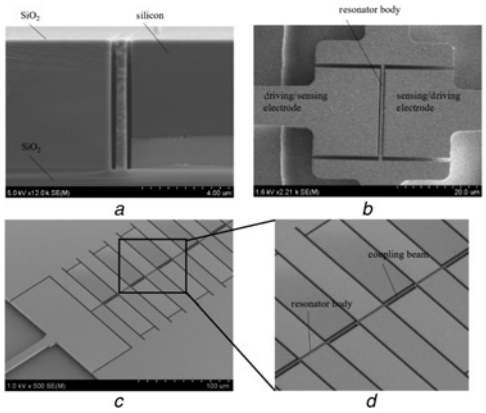

Fig. 4 *Fabricated results*
a Cross-sectional image of capacitive gaps after deep RIE
b Single capacitive silicon nanomechanical resonator
c Mechanically coupled capacitive silicon nanomechanical resonator
d Close-up image of mechanical coupled capacitive silicon resonator

nm-thick SiO_2 is grown on the SOI wafer by wet oxidation for the etching mask of the silicon device layer (Fig. 3*b*). On this SiO_2 layer, an electron beam (EB) resist (ZEP 520A) pattern is formed by EB lithography. Then, the SiO_2 layer is etched by reactive ion etching (RIE) using a gas mixture of CHF_3 and Ar with a power of 120 W and a chamber pressure of 5 Pa. The capacitive gap and resonator structures are formed by using deep RIE by Bosch process using SF_6 and C_4F_8 for short etching and passivation cycles (etching time 2.5 s, passivation time 2.5 s) for creating low scallops (Fig. 3*c*). The vertical sidewalls and small scallops of the capacitive gap are obtained as presented in Fig. 4*a*. The resonant body width and capacitive gap size are ~500 and 300 nm, respectively, as shown in Fig. 4*a*.

The structures of resonators on the SOI wafer will be transferred to a glass substrate by anodic bonding in order to reduce the parasitic capacitances from the handling silicon layer [21]. A 300 μm-thick Tempax glass has been prepared for anodic bonding with above wafer. Before bonding process, the top side of Tempax glass is partly etched in diluted HF using a metal mask (Cr–Au) (Fig. 3*d*). The SOI wafer and the Tempax glass are aligned and bonded together at 400°C with an applied voltage of 800 V for 15 min (Fig. 3*e*). The handling silicon layer of the SOI wafer is removed by plasma etching using SF_6 gas. The buried SiO_2 layer is etched out by a BHF solution. Finally, the Cr–Au films with thicknesses of 20 and 300 nm, respectively, are partly deposited by sputtering process via a stencil mask for electrode pads (Fig. 3*f*). The fabricated devices #1 and #2 are shown in Figs. 4*b* and *c*. Fig. 4*d* shows a close-up image of mechanical coupled capacitive silicon resonator.

3.2. Measurement setup: The measurement setup for the resonant characterisation of devices #1 and #2 is shown in Fig. 5. A

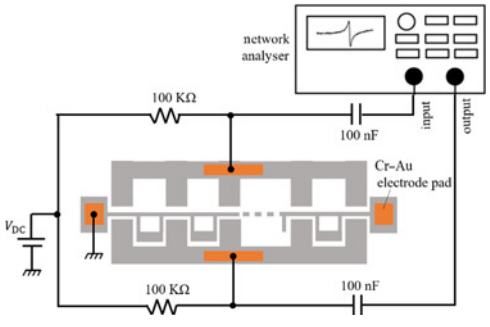

Fig. 5 *Measurement setup*

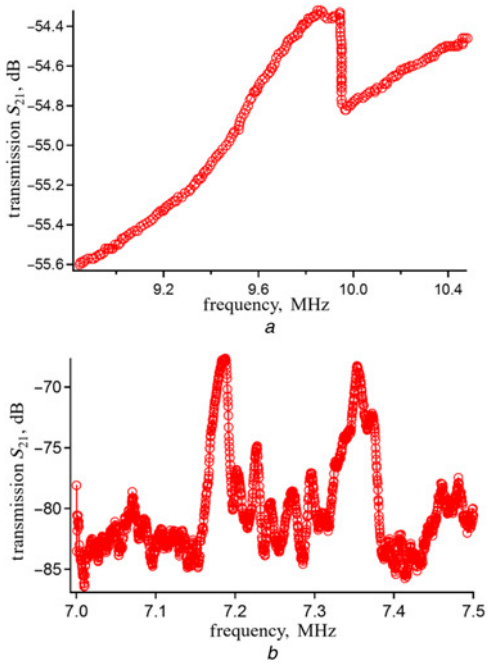

Fig. 6 *Frequency response of the fabricated devices*
a Single capacitive silicon nanomechanical resonator
b Mechanically coupled capacitive silicon nanomechanical resonator

network analyser (Anritsu MS4630B, Atsugi, Japan) with a frequency range from 10 Hz to 300 MHz has been employed for this evaluation. A DC voltage is applied to the driving and sensing electrodes against the grounded resonator body through a 100 kΩ resistor, which decoupled from the RF output of the network analyser using a 100 nF capacitor. The output of the devices is obtained by capacitive detection between the sensing electrode and the resonant body. Small changes in the capacitive gap generate a voltage on the RF input of the network analyser. The resonator is placed inside a vacuum chamber at 0.01 Pa with coaxial feed-through.

3.3. Measurement results: The resonant characteristics of the fabricated devices #1 and #2 are evaluated, as the specification is summarised in Table 1. The transmission S_{21} of device #1 is shown in Fig. 6*a* for a single resonator with a length of 21.3 μm, a width of 500 nm, a thickness of 5 μm and the capacitive gap size of about 300 nm. A resonant peak, which is observed under the measurement conditions $V_{DC} = 10$ V and $V_{AC} = 0$ dBm, is found at 9.9 MHz. Jump and drop phenomenon also arose in this device as shown in Fig. 6*a*. The amplitude of frequency response increases as the frequency is swept upward, and then suddenly jumps to a lower value. This hard spring effect of beam resonators has also observed in [9, 22]. The displacement goes beyond the ranges of small perturbations, tension is applied to the resonating structure and this makes it stiffer. This situation is identical to the hardening spring.

The resonant peaks of device #2 are found at around 7.2 MHz. The resonant peaks are clearly observed with the resonant amplitude of 20 dB and a high Q factor of 1000 is achieved for the nanomechanical resonators with a number of 100. The observed resonant frequency of device #2 is lower than that of device #1. It is in good agreement with the FEM simulation as mentioned before (Section 2). To evaluate the motional resistance of the coupling capacitive resonator, we assume the quality factor of coupling and single resonators are same. Based on the L, W, t, V_{DC} and assumed Q value and (1), the motional resistance of the single capacitive resonator without coupling is about 120 kΩ. In turn, the motional resistance of the mechanical coupling resonator of the number of 100 exhibits

about 1.2 kΩ calculated by (7). Some resonant peaks have been observed (Fig. 6*b*), which shows that most nanomechanical resonators are mechanically coupled and synchronised.

4. Conclusion: We designed, fabricated and evaluated the mechanically coupled capacitive silicon nanomechanical resonators to detect the small motional capacitance for attaining a low motional resistance towards high emerging sensing, image and data processing technologies. Resonant peaks can be observed, which shows that most nanomechanical resonators are mechanically coupled and synchronised.

5. Acknowledgments: Part of this work was performed in the Micro/Nanomachining Research Education Center (MNC) of Tohoku University, also performed in Junichi Nishizawa Memorial Research Center of Tohoku University. This work was supported in part by a Grant-in Aid for Scientific Research from the Japanese Ministry of Education, Culture, Sports, Science and Technology of Japan, also supported in part by Special Coordination Funds for Promoting Science and Technology, Formation of Innovation Center for Fusion of Advanced Technologies.

6 References

[1] Beek J.T.M.V., Puers R.: 'A review of MEMS oscillators for frequency reference and timing applications', *J. Micrmech. Microeng.*, **2012**, 22, p. 013001
[2] Toan N.V., Miyashita H., Toda M., *ET AL.*: 'Fabrication of an hermetically packaged silicon resonator on LTCC substrate', *Microsyst. Technol.*, 2013, **19**, pp. 1165–1175
[3] Gieseler J., Novotny L., Quidant R.: 'Thermal nonlinearities in a nanomechanical oscillator', *Nat. Phys.*, 2013, **9**, pp. 806–810
[4] Chaste J., Eichler A., Moser J., *ET AL.*: 'A nanomechanical mass sensor with yoctogram resolution', *Nat. Nanotechnol*, 2012, **7**, pp. 301–304
[5] Seo Y.J., Toda M., Ono T.: 'Si nanowire probe with Nd-Fe-B magnet for attonewton scale force detection', *J. Micrmech. Microeng.*, 2015, **25**, p. 045015
[6] Inomata N., Toda M., Sato M., *ET AL.*: 'Pico calorimeter for detection of heat produced in an individual brown fat cell', *Appl. Phys. Lett.*, 2012, **100**, p. 154104
[7] Rips S., Hartmann M.J.: 'Quantum information processing with nanomechanical qubits', *Phys. Rev. Lett.*, 2013, **111**, p. 049905
[8] Bannon F.D., Clark J.R., Nguyen C.T.C.: 'High Q factor HF micromechanical filters', *J. Solid-state Circuits*, 2000, **35**, pp. 512–526
[9] Mestron R.M.C., Fey R.H.B., Phan K.L., *ET AL.*: 'Experimental validation of hardening and softening resonances in a clamped-clamped beam MEMS resonator'. Proc. of the Eurosensor XXIII Conf., 2009, pp. 812–815
[10] Toan N.V., Kubota T., Sekhar H., *ET AL.*: 'Mechanical quality factor enhancement in a silicon micromechanical resonator by low-damage process using neutral beam etching technology', *J. Micromech. Microeng.*, 2014, **24**, p. 085005
[11] Toan N.V., Toda M., Kawai Y., *ET AL.*: 'A long bar type silicon resonator with a high quality factor', *IEE J. Trans. Sens. Micromach.*, 2014, **134**, pp. 26–31
[12] Lin Y.W., Li S.S., Xie Y., *ET AL.*: 'Vibrating micromechanical resonators with solid dielectric capacitive transducers gaps'. Proc. of IEEE Frequency Control Symp. and Exposition, 2005, pp. 128–134
[13] Toan N.V., Toda M., Kawai Y., *ET AL.*: 'A capacitive silicon resonator with movable electrode structure for gap width reduction', *J. Micrmech. Microeng.*, 2014, **24**, p. 025006
[14] Pourkamaki S., Ho G.K., Ayazi F.: 'Low impedance VHF and UHF capacitive silicon bulk acoustic wave resonators-part I: concept and fabrication', *IEEE Trans. Electron Devices*, 2007, **54**, pp. 2017–2023
[15] Sage E., Martin O., Dupre C., *ET AL.*: 'Frequency addressed NEMS arrays for mass and gas sensing applications'. Proc. of Transducers Conf., 2013, pp. 665–668
[16] Pourkamali S., Hashimura A., Abdolvand R., *ET AL.*: 'High Q single crystal silicon HARPSS capacitive beam resonators with self-aligned sub-100 nm transduction gap', *J. Microelectromech. Syst.*, 2003, **12**, pp. 487–496
[17] Jin Y., Tang Y., Yu X.: 'Study on clamped-clamped beams in-plane capacitive resonators'. Proc. of SPIE, 2009, vol. **7159**, pp. 71590P-1–71590P-8
[18] Durand C., Casset F., Ancey P., *ET AL.*: 'Silicon on nothing MEMS electromechanical resonator', *Microsyst. Technol.*, 2008, **14**, pp. 1027–1033
[19] Qishu Q., Pourkamali S., Ayazi F.: 'Capacitively coupled VHF silicon bulk acoustic wave filters'. Proc. IEEE Ultrason. Symp., 2007, pp. 1649–1652
[20] Demirci M.U., Abdelmoneum M.A., Nguyen C.T.C.: 'Mechanically corner-coupled square microresonator array for reduced series motional resistance', *J. Microelectromech. Syst.*, 2006, **15**, pp. 1419–1936
[21] Okada M., Nagasaki H., Tamano A., *ET AL.*: 'Silicon beam resonator utilizing the third-order bending mode', *Jpn. J. Appl. Phys.*, 2009, **48**, 06FK03-06FK03-8
[22] Husain A., Hone J., Postma H.C.Ch., *ET AL.*: 'Nanowire-based very high frequency electromechanical resonator', *Appl. Phys. Lett.*, 2003, **83**, pp. 1240–1242

doi: 10.1049/mnl.2016.0265